AL14 - The Magnetic Shielding Effect of Steel in an Aluminum Reduction Cell

Yiwen Zhou[1], Shouhui Chen[2] and Qingjie Zhao[3]
1. Senior Engineer
2. Senior Engineer
3. Professor
Zhengzhou Non-ferrous Metals Research Institute Co. ltd of CHALCO, Zhengzhou, China
Corresponding author: 20368266@qq.com

Abstract

Since several parts of an aluminum reduction cell are made of steel, their shielding effect on the distribution of magnetic field cannot be neglected. An electromagnetic finite element model of aluminum reduction cell was developed for this purpose. The magnetic fields of an aluminum reduction cell were analyzed with and without the shell and superstructure, cathode current collector bars or floor gratings. The results show that the vertical magnetic field (B_z) is strengthened at the upstream corners and alleviated at the downstream corners by the cathode current collector bars exits. While the shell has strong magnetic shielding effect, the floor grating and anode yokes and stubs have little magnetic shielding effect. On the other hand, the superstructure increases the magnetic field.

Keywords: Magnetic shielding effect, magnetic field distribution in aluminum reduction cell, finite element model.

1. Introduction

In an aluminum reduction cell, the direct current goes from busbars to anode rods, through carbon anodes, molten bath containing alumina and metal and carbon cathode to cathode collector bars. As the electrical current passes through the bath, the alumina is decomposed into molten aluminium (Al) and oxygen (O_2). The oxygen consumes carbon (C) in the carbon anode blocks and forms carbon dioxide (CO_2) which is later released to the exhaust gas system. The current then passes in cathode busbars to anodic busbars of downstream cell in the potline series of cells.

The magnetic field is generated by the electrical current that flows in the reduction cell. The relationship between the magnetic field contribution and its source current element follows the Biot-Savart law. The direction of the magnetic field follows the right-hand rule.

The third Maxwell's equation tells us that there are no magnetic charges, and therefore no sources and sinks for the magnetic field. All the field lines that enter through the surface into a volume enclosed by the surface also exit through another surface of the volume. Magnetic field lines are always closed loops. Unlike electricity, magnetic fields cannot be blocked or insulated, which makes shielding necessary. There is no way to block these field lines. Instead of attempting to stop these magnetic field lines, magnetic shielding re-routes them around an object. This is done by surrounding the device with a ferromagnetic material. Magnetic permeability describes the ability of a material to be magnetized. If the material used has a greater permeability than the object inside, the magnetic field will tend to flow along this material, instead of the objects inside.

Steel shell, superstructure, collector bars and floor grating are ferromagnetic materials in the reduction cell. Their permeability is much greater than that of other materials of the cell. Therefore, the magnetic field generated will tend to flow along those ferromagnetic parts.

The magnetic field produced by superposition of the different fields is responsible for the circulation of the metal, heaving and oscillation of the metal surface. Some of these phenomena have negative effect on the reduction process.

There are many works aiming to alleviate magnetic field by busbar configuration. Qi Xiquan [1] studied the influence of the bypassed cells and end cells on the magnetic fields. Li Mao [2] modeled the busbar configuration in aluminum reduction cells and made optimization with a genetic algorithm. Ziegler and Ruan [3] took partial account of the effect of the steel in automated optimization of the magnetic fields of the end cells.

Stephane Wan Tang Kuan et, al [4] studied the optimization of busbar design at the full smelter scale. A few designs [5-8] have been adopted to compensate for external magnetic fields with side risers. However, little attention has been devoted to the magnetic shielding effects of the ferromagnetic materials. To obtain a preferable magnetic field in the reduction cell, further studies are still necessary.

However, the irregular structure of steel complicates the magnetic field. The computation of ferromagnetic effect on the magnetic field distribution is generally expensive, because it involves a material non-linearity and interactions among the steel structures. The development of computers enables the finite element analysis of more ferromagnetic materials to be covered in the model than ever before.

The purpose of this paper is to investigate the influence of different parts of steel on the magnetic field using a finite element model of the whole cell. It is helpful for further studies on magnetic field optimization by steel configuration.

2. Mathematic Model

To obtain the magnetic effect of the aluminum reduction cell, the electric current and the induced magnetic field should be solved.

The current is solved by the Ohm's law, which governing equation is shown in Equation (1).

$$\mathbf{J} = -\sigma \nabla V \tag{1}$$

where:

J	Current density vector, A/m2,
V	Electric potential, V,
σ	Electrical conductivity, S/m.

For the whole cell, the current is conserved as Equation (2):

$$\nabla \bullet \mathbf{J} = 0 \tag{2}$$

Hence, using Equation (1) substitute **J**, Equation (2) turns into Laplace equation:

$$\nabla \bullet (\sigma \nabla V) = 0 \tag{3}$$

The initial magnetic field is calculated by Biot- Savart's law:

$$\mathbf{H}_g = \frac{1}{4\pi} \iiint_{vol} \frac{\mathbf{J} \times \mathbf{r}}{r^3} d(vol) \tag{4}$$

where:
Hg Initial magnetic field intensity vector generated by the source current (conductor), A/m.
vol Volume of the conductor, m^3
r Distance vector between the conductor and the target point, m

The relationship between the magnetic induction and the magnetic field intensity is calculated by the Equation (5).

$$\mathbf{B} = \mu\mathbf{H} \tag{5}$$

Where:
B Magnetic induction, Tesla
μ Magnetic permeability.

H is calculated by Equation (6).

$$\mathbf{H} = \mathbf{H}_g - \nabla\phi_g \tag{6}$$

where:
Φg is the magnetic scalar potential, which is calculated by Equation (7):

$$\nabla \bullet \mu\nabla\phi_g - \nabla \bullet \mu\mathbf{H}_g = 0 \tag{7}$$

3. Physical Model

An aluminum reduction cell of 350 kA is used as the physical model. The main specifications are listed in Table 1.

Table 1. Specifications of the reduction cell.

Parameter	Value	Parameter	Value
Line current	350 kA	Bath height	0.18 m
No. of anodes	48	Anode to side distance	0.30 m
Anode size	1.55×0.66×0.6 m	Anode to end distance	0.40 m
No. of cathodes	30	Anode cathode distance	0.042 m
Cathode size	3.34×0.52×0.45 m	Aluminum pad height	0.22 m
No. of stubs	4	No. of pillar	6
Stub diameter	0.135 m	Pillar size	2.882×0.45×0.36 m
Stub height	0.15 m	Anode beam	16.8×0.55×0.17 m
Rod size	1.5×0.2×0.17 m	Collector bar size	2.05×0.18×0.07 m

4. Finite Element Model

A finite element model of aluminum reduction cell was developed, in which, geometrically, the anode assembly, cathode assembly, bath, molten aluminum pad, side ledge, lining, shell, framework of superstructure, ground grating, busbar system and surrounding air are included.

The ground grating is commonly made of thin steel bars and it looks like a grid. It is possible to take the entire ground grating into the model, but the meshing work is time consuming. Furthermore, because of the crisscross along thin bars, meshing results in large amounts of elements that draw most of the computer resources or even beyond the computers' capacity for

large reduction cells. Therefore, the dimensions of thin steel bars of the ground grating are enlarged in the model. In order to minimize the total number of elements, various element sizes are used for different parts.

The busbar system in which the current flows from the cathode current collector bars to the anode rods of next cell was represented with the source current elements in the model.

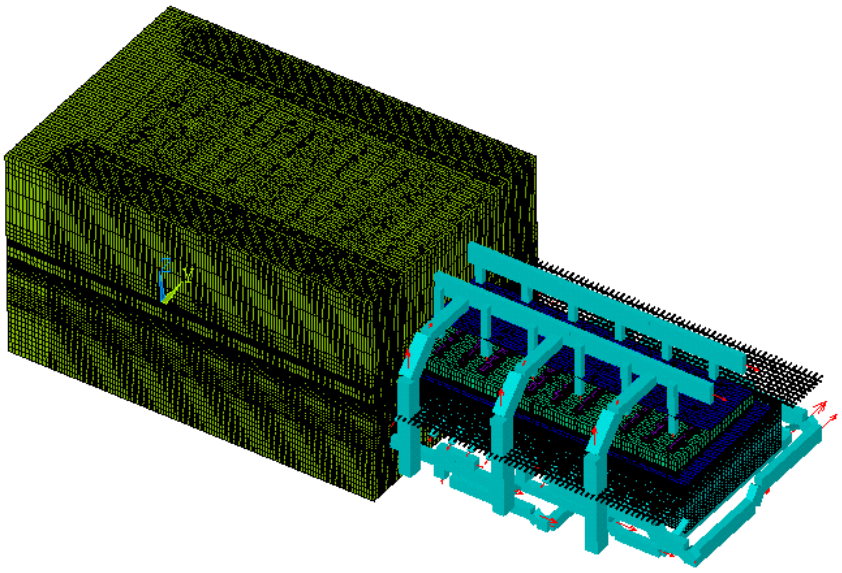

Figure 1. Finite element model.

Electrically, the top surfaces of yoke are assumed at a uniform electrical potential. We set the interfaces where the collector bars and busbar meet as a boundary condition of zero voltage and set the top surfaces of yoke as the current inlets.

Thermally, temperature is assumed constant throughout the whole model. Except the temperature of the collector bar ranges from low to high temperature, other steel materials are operated at moderate temperature. In order to simplify the question, the Curie temperature of the collector bars was not taken into account.

The model is made up to 2 248 781 elements for one cell with commercial code ANSYS. For each case, it takes about 20 hours to solve the model.

5. Results and Discussion

In the model, the direction from the center of the cell to the downstream of the cell is defined as Y direction, the direction from the center of the cell to tap end as X direction, and up vertical direction as Z direction. Among the three directions of the induced magnetic field, magnetic field in the Z direction (hereinafter referred to as B_z) in the metal pad is responsible for the metal waves when it interacts with the horizontal currents. Nevertheless, the results and discussion are focused on the B_z. It should be noted that the data points used for analyzing are not evenly distributed in space owing to the various element sizes. However, for all the cases, the same meshing scheme is used, which justifies the appropriateness of the analysis.

In order to find out the shielding effect of the steel parts, a cell model with carbon anode, carbon cathode, bath, molten aluminum pad, side ledge, lining, busbar system and surrounding air

included and without any steel is used as a base model. The models with steel parts added into step by step are solved separately.

5.1. Influence of Collector Bars

All current that flows in the cell electrical circuit will produce magnetic field. A base model without any ferrous material is solved, and the result of vertical component (B_z) of the magnetic field in the molten aluminum pad is shown in Figure 2, the distribution of magnitude B_z is listed in Table 2.

Table 2. Distribution of magnitude B_z without steel.

Range (Tesla)	B_z (number of data points)	B_z (%)
-0.011 - -0.01	1	0.00
-0.01 - -0.009	27	0.05
-0.009 - -0.008	189	0.34
-0.008 - -0.007	551	1.00
-0.007 - -0.006	1203	2.19
-0.006 - -0.005	2320	4.21
-0.005 - -0.004	2453	4.46
-0.004 - -0.003	3532	6.42
-0.003 - -0.002	8313	15.10
-0.002 - -0.001	4114	7.47
-0.001 - 0	4793	8.71
0 - 0.001	5059	9.19
0.001 - 0.002	4196	7.62
0.002 - 0.003	8832	16.05
0.003 - 0.004	3672	6.67
0.004 - 0.005	2986	5.42
0.005 - 0.006	1682	3.06
0.006 - 0.007	736	1.34
0.007 - 0.008	297	0.54
0.008 - 0.009	80	0.15
0.009 - 0.01	9	0.02
0.01 - 0.011	0	0.00

Without any steel in the model, the maximum absolute value of B_z magnitude is greater than 0.010 T and over 77 % of B_z is between -0.0040 and 0.0040 T, among which over 30 % of B_z is in ± (0.0020–0.0030) T. As shown in Figure 2, the magnitude of B_z is relatively big, and especially at the four corners. In the center of the cell, B_z is very small and close to zero. And the magnitude increases at the tap end and the duct end, while B_z is in opposite direction. When electricity flows in the long straight busbar, it creates a cylindrical magnetic field around the bar according to the right-hand rule. Hence, it could be deduced that most of B_z value is attributable to effect of horizontal busbar installed around the cell.

Collector bars are added to the base model. The B_z with collector bars in the model is shown in Figure 3 and the distribution of magnitude B_z is listed in Table 3. With collector bars (steel) in the model, the maximum of absolute value of magnitude B_z is over 0.011 T. More than 75 % of B_z is between -0.0040 and 0.0040 T, among which over 25 % of B_z is in ± (0.0020–0.0030) T. The numbers of data points in all range in Table 3 are different from those in Table 2. And the data points in Table 3 are distributed in a wider range than those in Table 2. The collector bars

are parallel to each other and the currents pass through the collector bars horizontally. Therefore, the magnetic field generated by collector bars is counteracted by those generated by neighboring collector bars. However, there are less counteracted parts for the magnetic fields generated by collector bars at the duct end or tap end. Hence, when compared with the B_z in the Figure 1, the B_z in the Figure 2 at the corners of current upstream (right upper corner) is strengthened, and the B_z at the corners of current downstream (left down corner) is alleviated.

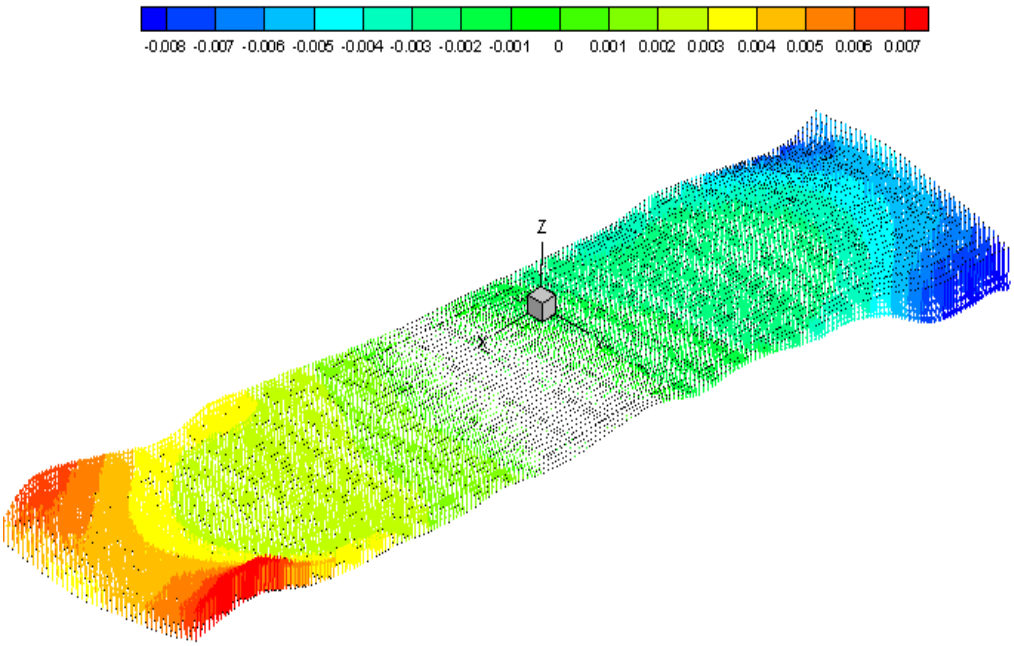

Figure 2. The direction and magnitude of B_z without ferrous materials in the model.

Table 3. Distribution of B_z magnitude with collector bars.

Range (Tesla)	B_z (number of data points)	B_z (%)
-0.012 - -0.011	13	0.02
-0.011 - -0.01	55	0.10
-0.01 - -0.009	134	0.24
-0.009 - -0.008	293	0.53
-0.008 - -0.007	653	1.19
-0.007 - -0.006	1290	2.34
-0.006 - -0.005	2450	4.45
-0.005 - -0.004	2354	4.28
-0.004 - -0.003	3319	6.03
-0.003 - -0.002	6688	12.15
-0.002 - -0.001	5247	9.53
-0.001 - 0	4877	8.86
0 - 0.001	5405	9.82
0.001 - 0.002	5308	9.64
0.002 - 0.003	7092	12.88
0.003 - 0.004	3416	6.21
0.004 - 0.005	3135	5.70
0.005 - 0.006	1773	3.22
0.006 - 0.007	900	1.64

0.007 - 0.008	399	0.72
0.008 - 0.009	161	0.29
0.009 - 0.01	65	0.12
0.01 - 0.011	18	0.03

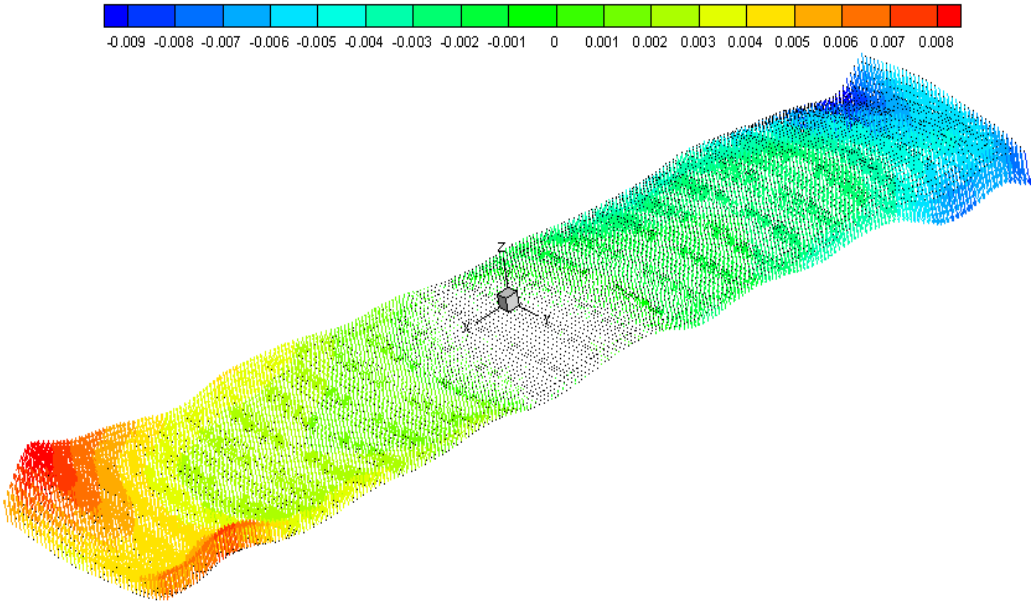

Figure 3. The direction and magnitude of B_z with collector bars in the model.

5.2. Influence of the Shell

Besides the collector bars, the shell is added into the model. The magnetic result (B_z) of this model is shown in Figure 4. Apparently, the magnitude of B_z is much smaller than those in Figure 2 and Figure 3. The maximum absolute value of B_z decreases from 11.8 mT to 3.3 mT, and the average absolute value of B_z decreases from 2.7 mT to about 0.3 mT. 97 % of B_z is between -0.0010 and 0.0010 T. The shell is similar to a steel box without top face. Hence, most of the magnetic field generated by the busbars which lay outside of the shell is blocked by the steel shell.

Table 4. Distribution of B_z magnitude with shell.

Range (Tesla)	B_z (number of data points)	B_z (%)
-0.006 - -0.005	0	0.00
-0.005 - -0.004	0	0.00
-0.004 - -0.003	6	0.01
-0.003 - -0.002	124	0.23
-0.002 - -0.001	700	1.27
-0.001 - 0	34073	61.90
0 - 0.001	19610	35.63
0.001 - 0.002	445	0.81
0.002 - 0.003	84	0.15
0.003 - 0.004	3	0.01
0.004 - 0.005	0	0.00
0.005 - 0.006	0	0.00

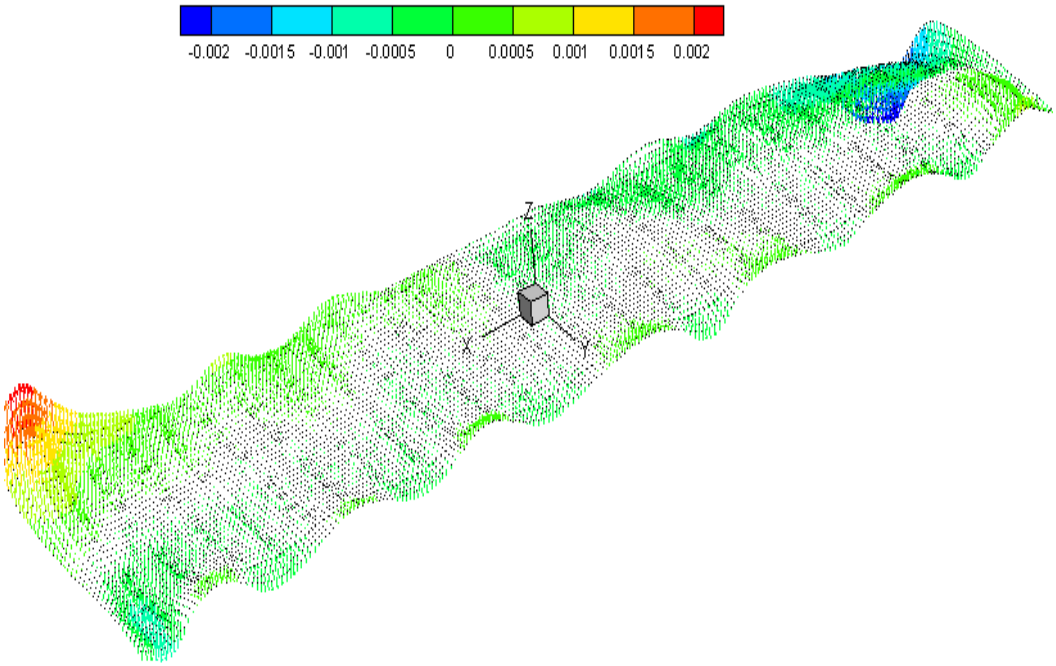

Figure 4. The direction and magnitude of B_z with shell in the model.

5.3. The Influence of Yokes and Stubs

Through the yokes and stubs, the current is evenly distributed in the anodes. Due to the presence of the collector bars and the shell, the electromagnetic model with yokes and stubs is solved. The magnitude and direction of B_z in the metal pad is shown in Figure 5.

Table 5. Distribution of B_z magnitude with yokes and stubs.

Range (Tesla)	B_z (number of data points)	B_z (%)
-0.005 - -0.004	0	0.00
-0.004 - -0.003	5	0.01
-0.003 - -0.002	95	0.17
-0.002 - -0.001	566	1.03
-0.001 - 0	32791	59.57
0 - 0.001	21188	38.49
0.001 - 0.002	336	0.61
0.002 - 0.003	62	0.11
0.003 - 0.004	2	0.00
0.004 - 0.005	0	0.00

There is no apparently difference between the Figure 4 and Figure 5. 98 % of B_z is between -0.0010 and 0.0010 T. The data infers that the difference of averaged absolute B_z between the model with s is only 0.0001 Tesla (0.1 mT), which indicates that the yokes and stubs in the model make tiny difference on the magnetic field. The averaged current in stubs and yokes is small owing to the evenly distributed current in all the stubs and yokes. The current in the stubs is vertical. Therefore, little change of magnetic field B_z is made in the aluminum pad.

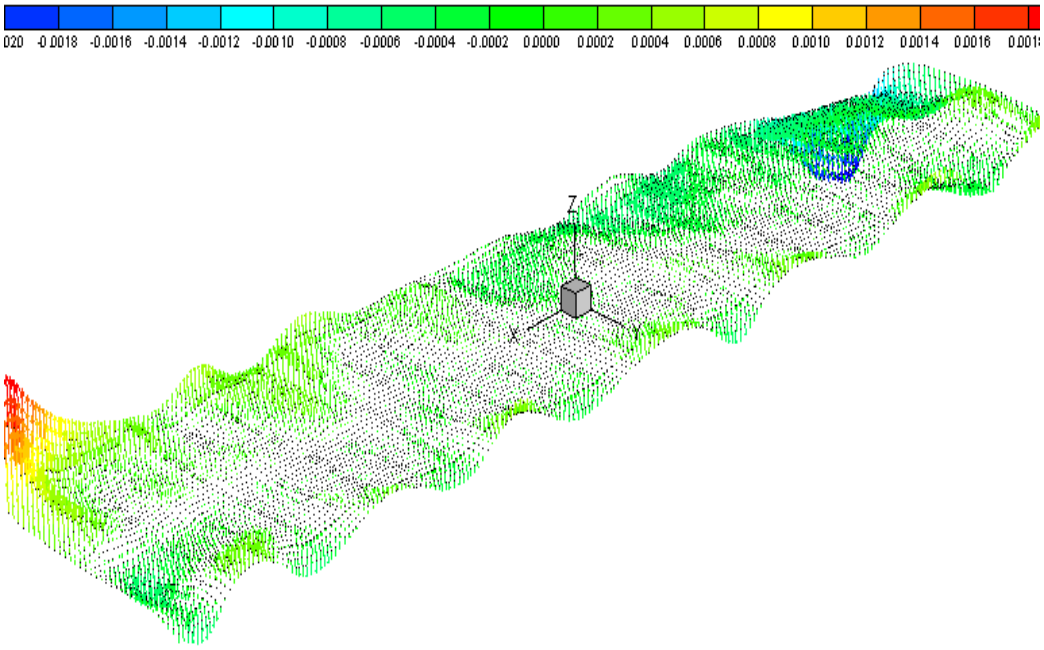

Figure 5. The direction and magnitude of B_z with yokes and stubs in the model.

5.4. Influence of the Superstructure

The superstructure occupies quite a large space over the cell. Except for the insulations, it is made of steel. It can be simplified as three steel plates; two steel plates spaced vertically sit on one horizontal steel plate. With the collector bars, shell, yokes and stubs present, the result of electromagnetic model with superstructure is shown in Figure 6. Compared with the previous model, B_z between -0.0010 and 0.0010 T decreased from 98 % to 86 %.

Due to the the superstructure, the magnitude of B_z at both tap end and duct end increases, while little change happens in the middle part. The result indicates that the superstructure attenuates the shielding effect of the shell, mainly because of the steel's bigger relative permeability. As for magnetic field lines, the superstructure is the shortcut that will draw part of the magnetic field lines originally from upper space to pass through. Consequently, the magnetic field in the nearby metal pad is changed little.

Table 6. Distribution of B_z magnitude with superstructure.

Range (Tesla)	B_z (number of data points)	B_z (%)
-0.005 - -0.004	0	0.00
-0.004 - -0.003	7	0.01
-0.003 - -0.002	173	0.31
-0.002 - -0.001	5411	9.83
-0.001 - 0	22304	40.52
0 - 0.001	25036	45.48
0.001 - 0.002	2013	3.66
0.002 - 0.003	98	0.18
0.003 - 0.004	3	0.01
0.004 - 0.005	0	0.00

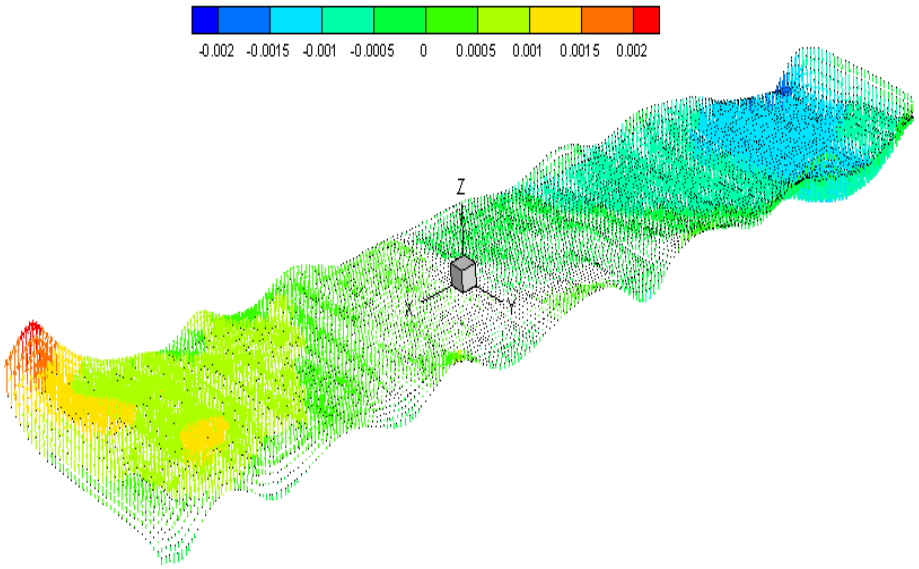

Figure 6. The direction and magnitude of B_z with superstructure in the model.

5.5. Influence of the Floor Grating

Having taken the collector bars, shell, yokes, stubs and superstructure into account, the result of electromagnetic model with floor grating is shown in Figure 7. Due to the existence of gratings, the magnitude of Bz of metal pad changes a little bit, numerically about one 0.1 mT. In the model, the grid of floor grating is much bigger than it actually is that results in large magnetic leakage. In reality, the actual floor grating has better shielding effect than this result presented. A model with actual floor grating may be presented with a more powerful computer in the future.

Table 7. Distribution of B_z magnitude with floor grating.

Range (Tesla)	B_z (number of data points)	B_z (%)
-0.005 - -0.004	0	0.00
-0.004 - -0.003	3	0.01
-0.003 - -0.002	139	0.25
-0.002 - -0.001	5056	9.19
-0.001 - 0	22623	41.10
0 - 0.001	25426	46.19
0.001 - 0.002	1722	3.13
0.002 - 0.003	75	0.14
0.003 - 0.004	1	0.00
0.004 - 0.005	0	0.00

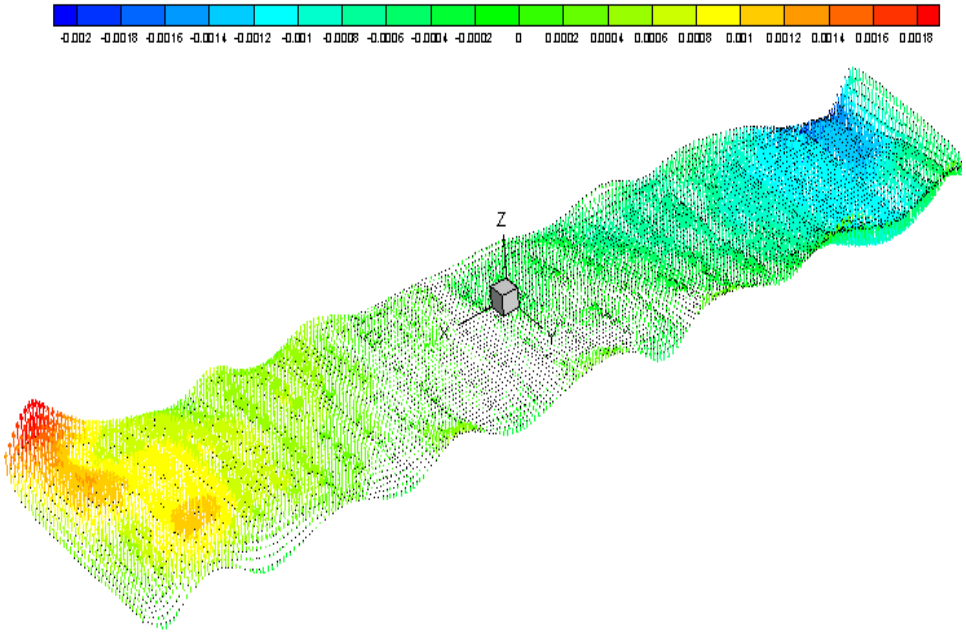

Figure 7. The direction and magnitude of B_z with ground grating in the model.

6. Conclusions

The magnetic shielding effect of the steel parts was analyzed. The results showed that each part has different magnetic shielding effect for the aluminum pad in the cell. If there were no steel in the cell, the magnitude of B_z would be relatively large. Most of the magnetic field generated by the outside busbars is shielded by the shell and little is shielded by the ground grating. The collector bars have some influence on B_z at four corners of the cell. The yokes and stubs have little influence on the magnetic field. However, the superstructure brings more magnetic lines through the metal pad.

In order to lower the B_z in the metal pad, more efforts could be directed on the design of the shell and superstructure for a given busbar system.

7. References

1. Qi Xiquan, Study on the influences of potline status on the magnetic fields of aluminum reduction cells, *Light Metals* 2011, 859-63.
2. Li Mao, Zhou Jiemin, Modeling and optimization of busbar configuration in aluminum electrolysis cells with genetic algorithm, *Light Metals* 2010, 489-92.
3. Donald P. Ziegler, Yimin Ruan, Busbar arrangement optimization for end cells, *Light Metals* 2009, 535-38.
4. Stephane Wan Tang Kuan, Denis Jacquet. Optimization in magnetic modeling, *Light Metals* 2008, 397-402.
5. Donald P. Ziegler, Stability of metal/electrolyte interface in Hall-Héroult cells: Effect of the steady velocity, *Metall. Trans. B*, 1993, vol. 24(5), 899-906.
6. M. Li and J. M. Zhou, Numerical simulation of busbar configuration in large aluminum electrolysis cell. *J. Cent. S. Univ.*, 2008, vol. 15(2), 271-75.
7. Marc Dupuis and Valdis Bojarevics. Busbar sizing modeling tools: comparing an ANSYS® based 3D model with the versatile 1D model part of MHD-Valdis[C]. *Light Metals 2006*, 341-46.
8. Thorleif Sele. Instabilities of the metal surface in electrolytic alumina reduction cells[J]. *Metall. Trans. B*, 1977, vol. 8B, 613-18.